Received: 19 May 2022 | Revised: 15 September 2022 | Accepted: 4 October 2022

DOI: 10.1002/pro.4464

FULL-LENGTH PAPER

THE PROTEIN SOCIETY WILEY

Copper coordination states affect the flexibility of copper Metallochaperone Atox1: Insights from molecular dynamics simulations

Renana Schwartz | **Sharon Ruthstein** | **Dan Thomas Major**

Department of Chemistry and Institute for Nanotechnology and Advanced Materials, Bar-Ilan University, Ramat-Gan, Israel

Correspondence
Sharon Ruthstein, Department of Chemistry and Institute for Nanotechnology and Advanced Materials, Bar-Ilan University, Ramat-Gan 5290002, Israel.
Email: sharon.ruthstein@biu.ac.il

Dan Thomas Major, Department of Chemistry and Institute for Nanotechnology and Advanced Materials, Bar-Ilan University, Ramat-Gan 5290002, Israel.
Email: majort@biu.ac.il

Funding information
Israel Science Foundation, Grant/Award Number: Grant # 1683/18

Review Editor: Nir Ben-Tal

Abstract

Copper is an essential element in nature but in excess, it is toxic to the living cell. The human metallochaperone Atox1 participates in copper homeostasis and is responsible for copper transmission. In a previous multiscale simulation study, we noticed a change in the coordination state of the Cu(I) ion, from 4 bound cysteine residues to 3, in agreement with earlier studies. Here, we perform and analyze classical molecular dynamic simulations of various coordination states: 2, 3, and 4. The main observation is an increase in protein flexibility as a result of a decrease in the coordination state. In addition, we identified several populated conformations that correlate well with double electron–electron resonance distance distributions or an X-ray structure of Cu(I)-bound Atox1. We suggest that the increased flexibility might benefit the process of ion transmission between interacting proteins. Further experiments can scrutinize this hypothesis and shed additional light on the mechanism of action of Atox1.

KEYWORDS

Atox1, copper-binding, molecular dynamics, molecular simulations, protein flexibility

1 | INTRODUCTION

Copper is an essential element for proper cell function but may be toxic at high, unregulated concentrations.[1] Copper ions access eukaryotic cells from the blood via copper transport proteins like Ctr1.[2,3] Subsequently, the ions are transmitted to metallochaperones like Atox1[4] that carry the ions to ATPases like ATP7A and ATP7B (Menkes and Wilson disease proteins, respectively).[5]

Atox1 is a small and soluble intracellular chaperone protein, composed of only 68 amino acids. It includes the overall structure of βαββαβ while the preserved Cu(I) binding motif of MXCXXC lay at the N-terminus of the larger helix (α1) (see Figure 1).[5] A similar motif is also found in the target ATPases. The interactions with the intracellular domain of the Ctr1 protein are less known. It has been speculated that the wealth of positively charged residues (mainly Lys56, Lys57, Lys60, but also Arg21 and Lys25) might facilitate interaction between the Atox1 monomer and negatively charged lipid headgroups while the Cu(I) binding residues point in the proper direction and thus facilitate Cu(I) transfer.[6]

Abbreviations: ABNR, adopted basis Newton–Raphson; AMBER, Assisted Model Building with Energy Refinement; CHARMM, chemistry at Harvard macromolecular mechanics; DEER, double electron–electron resonance; DNA, deoxyribonucleic acid; EPR/ESR, electron paramagnetic/spin resonance; FF, force field; HF, Hartree–Fock; MD, molecular dynamics; MM, molecular mechanics; MTSL, S-(1-oxyl-2,2,5,5-tetramethyl-2,5-dihydro-1H-pyrrol-3-yl)methyl methanesulfonothioate; NAMD, nanoscale molecular dynamics; PBC, periodic boundary conditions; PDB, Protein Data Bank; QM, quantum mechanics; RMSD, root-mean-square deviation; RMSF, root-mean-square fluctuation.

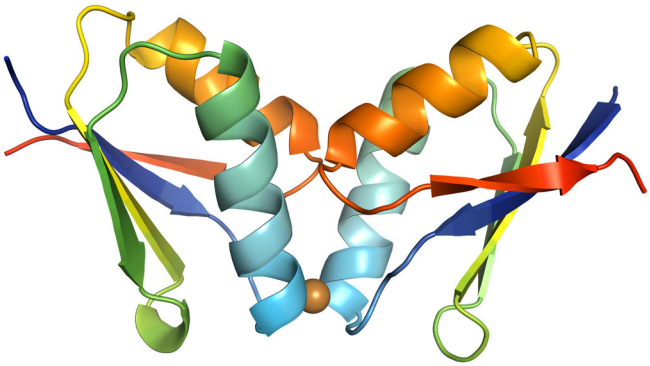

FIGURE 1 Homodimer of Atox1 (PDB 1FEE)

A reported crystal structure of Atox1 included a dimer version where the copper ion is bound to four Cysteine residues (Cys12 and Cys15 of each chain).[5] Atox1's structure has a dual role: on the one hand, it must bind the metal ion tightly while transporting it, and on the other hand, it has to properly interact with other partner proteins for metal transfer.[7,8] One possible property of Atox1 which assists those processes is its great flexibility and its ability to adopt different conformations. A recent study on Atox1, employing double electron–electron resonance (DEER) measurements, showed complex distance distributions with a wealth of peaks related to several positions in the dimer.[9] In addition, another study employed hybrid quantum mechanics-molecular mechanics (QM/MM) and molecular dynamics (MD) methods to investigate the copper binding in Atox1.[10] In this work, the relevant copper-binding residues and the Cu(I) ion itself were treated as QM while the rest of the system was calculated using MM. The QM/MM MD calculations enabled addressing directly which coordination state is preferable in the dimeric state, similarly to previous computational predictions for the monomeric Atox1.[11,12] In these dimeric Atox1 simulations, transitions between 4- and 3-coordinated states were seen, although the 4-coordinated state dominated. A 2-coordinated state was only observed as a fleeting state. Due to the cost of QM/MM simulations, it was not possible to observe any large-scale protein motions.

In the present study, we employ MM MD simulations to model the three coordination states explicitly, allowing significantly longer simulations. MM MD simulations with the Cu(I) ion require suitable force field (FF) parameters. In this work, we developed specific FF parameters to describe the binding between the Cu(I) ion and varying number of cysteine residues, extending a previous work that dealt with a 2-coordinated system of a different Bacterial metalloregulator, CueR.[13] Recent experiments with spin-labeled DNA showed that the CueR protein can bend DNA with and without Cu(I) ions (although a higher concentration of protein is required without Cu(I)).[14] This supports the observation of bending and twisting motions both in Cu(I) bound (holo) and unbound state (apo) in MD simulations of CueR.

In the case of Atox1 it was shown both experimentally (using specific Atox1 mutants) and computationally that residues Cys15 are bound more loosely to the Cu(I) ion compared with the Cys12 residues.[10,15] Yet, the copper binding via Cys15 stabilizes the dimeric form of Atox1. Following these findings, the Cys12 residues coordinate copper in all models (2-, 3-, and 4-coordinated), while one or two of the Cys15 residues were defined as coordinating copper to achieve the desired binding mode (3- or 4-coordinated). Using MM MD simulations, we observed increased flexibility in the low coordination state, while the 4-coordination state was quite rigid during the ~0.5 μs simulation time. The 2-coordinated state was the most flexible and displayed various conformations which mainly differ by the relative orientation of the two subunits of Atox1. Using tools for predicting DEER distance distributions we identified several possible open conformations of the Atox1 protein that may contribute to the complex electron paramagnetic resonance (EPR) spectra.

2 | COMPUTATIONAL METHODS

Here, we conducted and analyzed brute-force MD simulations of the human metallochaperone Atox1 under different conditions. The dynamics of three different coordination states were each modeled and calculated using two different force fields (CHARMM- or AMBER-based, see details below).

We performed MD simulations at constant particle, pressure, temperature (NPT) conditions with explicit solvent using two force fields: the CHARMM36m force-field[16–18] and the AMBER 2014SB force-field,[19] using available topology and parameter files in the CHARMM program format.[20,21] The NAMD program[22,23] was used for the MD production runs. In each force field, the protein was modeled in three different coordination states: 2-, 3-, and 4-coordinated, where the numbers denote how many cysteine residues were bound to the Cu(I) ion. Three replicas were created for each state in each FF, differing in the initial assigned velocities, resulting in 18 independent runs. The details are described below.

2.1 | System construction

The initial structures for the simulations were prepared as follows: most of the residues were taken from the

PDB, entry 1FEE (dimeric Cu(I)-bound Atox1).[5] A few residues (Met1 of chain A and Glu68 of chain B) were added manually using the Maestro and PyMOL software packages (Schrodinger, Inc.). Hydrogens were added using the HBUILD facility in CHARMM.[20,21]

2.2 | FF Cu(I) parameters

The FF parameters describing the metal binding loop were developed based on three model systems: $[(CH_3S)_nCu(I)]^{(n-1)-}$; $n = 2, 3, 4$.[24] The geometry, vibrational modes, and rotational potential energy profiles for these models were calculated using the Gaussian 16 program, with the MP2 post-HF method and the aug-cc-pVTZ basis set.[25–28] The same model was defined in the CHARMM program, and minimized and subjected to vibrational frequency calculations. The geometric parameters and vibrational force constants obtained for use with CHARMM36m were gradually adjusted by modifying the FF parameters to achieve an optimal fit with the QM results (for final parameters, see Table S1). Parameters were also slightly adjusted and validated (by means of geometry and vibrational frequencies) to fit the AMBER FF. Numerical values for parameters and comparison with QM data appear in Tables S1 and S2 and in Figures S1 and S2. For distributions of some angles, torsional and improper torsional angles around the Cu(I) binding site during the simulations, see Figure S3.

2.3 | Setup of the solvated system

Using the CHARMM program,[20,21] the protein was placed in a cubic water (TIP3P) box of size ~80^3 Å^3 or ~65^3 Å^3 (see Table S3), and ions (Na^+, Cl^-) were added to neutralize the total charge and to mimic the experimental buffer concentration (lysis buffer, 25 mM Na_2HPO_4, 150 mM NaCl).[9] For details regarding the number of ions added, see Table S3. A gradual minimization of the water molecules and the ions was performed, followed by a short MD simulation and another minimization. The protein was fixed during this procedure. Subsequently, a restrained minimization of the protein was performed, with the force constants on the protein's heavy atoms reduced in a stepwise manner from 100 to 0 kcal mol^{-1} Å^{-2}. When using the CHARMM force field, we performed 1,650 ABNR minimization steps in the CHARMM program, while when using the AMBER force field, we performed 1,650 NAMD *minimize* steps.

2.4 | Free MD simulations

Following system preparation and relaxation, we moved our protein systems to the NAMD program,[22,23] which is faster than CHARMM, and can use the CHARMM FF, as well as CHARMM topology and parameter files directly without any modifications. AMBER SB14 files in CHARMM format were used, and two atom types were renamed to match NAMD conventions ("2C" and "3C" were renamed to "C2" and "C3," respectively). Three different replicas were modeled for each state in each FF, to obtain statistically significant data.[29] These replicas are named "Cu_*n*_x_ff," where *n* denotes coordination (2–4), x denotes replica number (i, ii, or iii), and ff denotes force field (CHARMM or AMBER).

The systems were gradually heated from 50 to 300 K over 30 ps (an increase of 50 K every 5 ps), followed by an equilibration phase of 2 ns. During this phase, the Cα atoms were gently restrained to their initial positions with a force constant of 1.0 kcal mol^{-1} Å^{-2}. These restraints were removed before moving to the free MD phase. This allows the heat to flow through the system until equilibration is reached, while avoiding loss of important structural features. Subsequently, we performed a free periodic boundary MD simulation at NPT conditions for 0.52 or 1.00 μs for each replica (see Table S3), for a total of 12.24 μs. These simulation replicas and times are considered sufficient to learn about protein motions at this time scale in cases where the replicas show convergent behavior. In addition, since we aimed to observe the true unperturbed dynamics of the system, brute force MD simulations are suitable. For CHARMM-based FF simulations, nonbonded interactions were smoothly switched off at 12–14 Å with a full electrostatic evaluation done every other step using the Particle Mesh Ewald method.[30] The Particle Mesh Ewald method for full electrostatics was used with a direct space tolerance of 10^{-6}, grid size of 64 (in ~65^3 Å^3 box) or 81 (in ~80^3 Å^3 box) and maximum grid spacing of 1.04 Å (1.1 Å for heating). The time step was 2 fs, which required the constraining of all covalent bonds involving hydrogen atoms to their equilibrium distance (ShakeH algorithm) with a tolerance of 10^{-8} Å.[31] Pressure and temperature were controlled by means of Langevin baro- and thermostats, with a damping coefficient of 1 ps^{-1}.[32] The hydrogens were not coupled to the heat bath. The pressure was calculated using hydrogen-group-based pseudo-molecular virial and kinetic energy, which is required when using SHAKE. The target pressure was 1 atm, kept by a Langevin piston with an oscillation period of 100 fs, and decay of 50 fs. Following standard AMBER methodology, some non-bonded definitions

were different for these simulations: no switching function was applied, and 1–4 interactions were scaled by 1.0/1.2.

2.5 | Trajectory analysis

Alignment of the frames with respect to the initial structure was performed prior to the analysis. All residues were used for the alignment. RMSD and RMSF (root-mean-square deviation and fluctuation) and characteristic angle values were calculated using the CHARMM software. The characteristic angle was defined by the following three atoms: Cα of $G27_A$, Cu(I), and Cα of $G27_B$. The residue chosen for this purpose, G27, is the C-cap of the large helix, while the Cu(I) is located near the N-terminus of this helix. RMSD-based clustering and PC analysis were performed using the R package Bio3D from the Grant lab.[33] In the process of clustering, as the number of clusters increases, statistically less relevant clusters (i.e., small) are generated. To avoid this, we defined a threshold, where no more than **either** ~30% of the clusters each accounted for less than 5% **or** ~40% of the clusters each accounted for less than 10% of the simulation time. Specifically, for this analysis, the δ (time interval between trajectory frames) was set to 0.2 ns. This analysis reveals long-range structural changes, so a relatively large delta is sufficient. For clustering, the preceding alignment and RMSD calculations were only performed for the Cα atoms in α-helices and β-sheets. After the clusters were defined, an average structure for each cluster was calculated, and this time, all atoms were considered. In addition, information about the number of frames assigned to each cluster and about its spread over time was collected (see Figure S4). Subsequently, we identified the instantaneous structure from the trajectory that was most similar to the cluster centroid, and this structure was used in subsequent DEER analysis.

2.6 | DEER facilitator

The structures most similar to the representative states were uploaded to the DEER Spin-Pair Distributor in the DEER facilitator on the CHARMM-GUI server.[34,35] The Cu(I) ion was omitted since the webserver did not have FF parameters for this ion.

To evaluate the dynamics of the spin label, a short minimization (500 ABNR steps), followed by a 10 ns-long MD simulation, was performed, with only the dummy spin labels free to move. To implicitly account for Brownian motion of other sidechains, these are treated as Alanine residues (except for Glycine residues). In this way, the starting conformations of the sidechains do not restrict the mobility of the spin label. The web server also enables the creation of a histogram of the distance between the dummy spin labels along with a list of the distance as a function of time. From these lists, the average values were calculated using Python and the NumPy library, along with their standard deviations.[36]

3 | RESULTS AND DISCUSSION

3.1 | Root-mean-square deviation

To assess the stability of the simulations and roughly estimate the conformational changes we computed the RMSD of the instantaneous structures with respect to the initial structure.[37] Figure 2a,d shows the RMSD plots of Cα atoms compared to the initial structure.

The Cα RMSD plots (Figure 2) for the various replicas and coordination states show significant differences in the MD trajectories as a function of the coordination state, as well as the replica. In the 4-coordinated state, we observe low RMSD values (< ~3 Å for AMBER-SB14, < ~5 Å for CHARMM36m), indicating small structural changes. In the 3-coordinated state we see higher RMSD values, sometimes including transitions to states with higher RMSD values (~4.5 Å [AMBER-SB14]; ~7 Å or ~ 10.5 Å [CHARMM36m]). Most of the 2-coordinated states sampled conformations with high RMSD values and some converged to a steady value (10–12 Å for CHARMM36m; 11 or 13.5 Å for AMBER-SB14). These RMSD values point to a relation between Cu-coordination number and protein flexibility, which is seen either as a sharp transition to alternative conformations or sampling a wealth of fleeting conformations. An additional key conclusion from the RMSD plots (Figure 2a,d) is the importance of performing MD simulations with several replicas. Here, we see that the three replicas of each coordination state differ, especially for the 2 and 3-coordination states, although the general conclusion regarding increased flexibility for the lower-coordinated replicas remain. We note that in our previous QM/MM study of Atox1, we observed greater flexibility for the 3-coordinated state compared to the 4-coordinated state, in agreement with the current findings.[10]

3.2 | Root-mean-square fluctuations

In the previous section, the behavior of the system as a function of simulation time was discussed. RMSF measures supply a different point of view, as it measures the time-average fluctuations of each residue (or Cα atom).[38] The RMSF plots (Figure 2b,c,e,f) show increased values

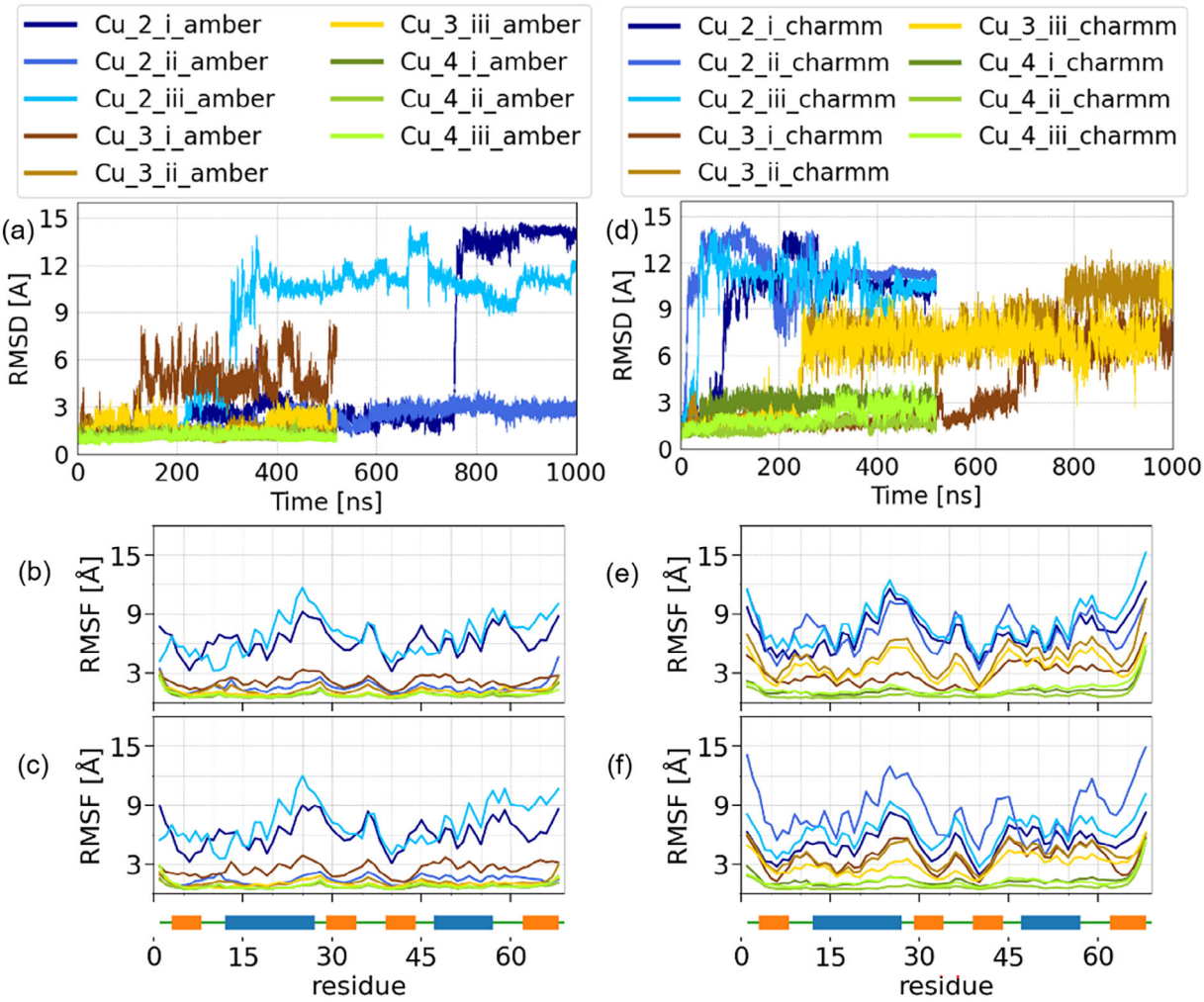

FIGURE 2 Root-mean-square deviation (RMSD) and root-mean-square fluctuation (RMSF) plots for CHARMM36m and AMBER SB14 FF trajectories. (a, d) RMSD values of Cα atoms as a function of simulation time for (a) AMBER-based replicas (d) or CHARMM-based replicas. Reference structure is the initial structure. (b, c, e, f) RMSF values of Cα atoms of each residue in chain A (Upper part: b, e) or B (lower part: c, f). Secondary structure guide appears below: Green: random coil; Orange: β-sheet; Blue: α-helix. Force fields: AMBER-based on the left (b, c); CHARMM-based on the right (e, f)

for flexible residues and agree with RMSD plots in terms of the trends observed as a function of the coordination state. The trend of increased mobility is clear for the CHARMM36m replicas but is less pronounced for the AMBER-SB14 replicas in the 3-coordinated state. In both cases, the loops and termini regions are characterized with higher values relative to the secondary structure elements. The increased RMSD and RMSF values for lower coordination states probably arise from enhanced flexibility around the copper hinge.

3.3 | Mutual RMSD-based clustering

The clustering process enables us to identify key conformations from the myriad of instantaneous conformations in the MD trajectories. The clustering analysis reveals numerous conformations for the 2-coordinated replicas, less for the 3-coordinated replicas, and a set of very similar structures for the 4-coordinated replicas. Some selected snapshots of the conformers are shown in Figure 3. In general, the opening and twisting process observed in the 2-coordinated state, and to a lesser degree in the 3-coordinated state, involves a butterfly motion of the 2 monomers. The most common configurations for the 2-coordinated states obtained using the CHARMM36m FF are twisted conformations. Among the 2-coordinated replicas obtained using AMBER-SB14, one presented an inverted conformation, one a closed conformation, and one a twisted conformation as in CHARMM36m replicas. The 3-coordinated replicas ranged from quite closed conformations (AMBER-SB14) to

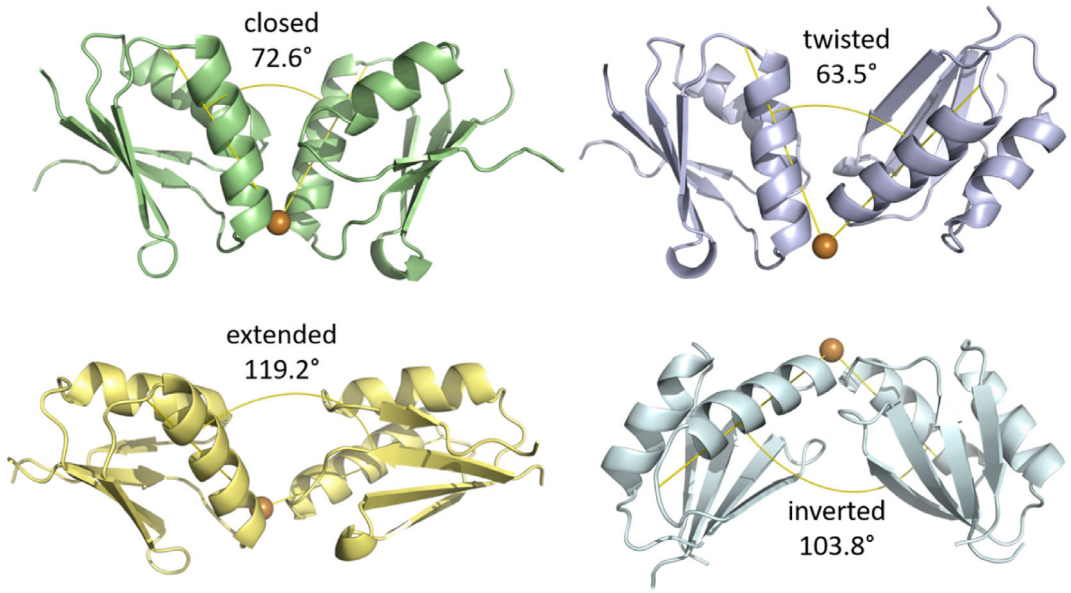

FIGURE 3 Main conformations of various coordination states: Closed conformation typical to 4-coordinated replicas, and using AMBER-SB14 also for 3-coordinated and one of the 2-coordinated replicas. Extended conformation typical to CHARMM36m 3-coordinated replicas. Inverted conformation observed in one of the AMBER-SB14 2-coordinated replicas. Twisted conformation typical to CHARMM36m 2-coordinated replicas and one of the AMBER-SB14 2-coordinated replicas. These conformations were used for double electron–electron resonance (DEER) predictions and their results generally agree with experiments. For more details see Table S4 and relevant sections

extended conformations (CHARMM36m). Even the closed conformations were more flexible and open than the 4-coordinated states. The 4-coordinated states remained closed throughout the simulations. To better understand the structural relation between different protein conformations, we performed principal component analysis (PCA). The PCA analyzes (Figure S5) show gradual transitions between the different states in the PC1/PC2 space for the 2-, 3-, and 4-coordinated systems. The cluster analysis reflects the increased flexibility quantitatively assessed by the RMSD/RMSF measures. It is also important to note that the secondary structural elements were mostly stable, and the conformational changes were dictated by the flexibility or rigidity of the copper binding hinge. The wealth of states seen in Figure 3 suggests that Atox1 can adopt multiple states in its low coordination states to interact with other Cu-binding proteins to facilitate metal ion transport. Recent work has shown a connection between Cu(I) binding and flexibility of the human copper-transporting protein ATP7B which interacts with Atox1.[39]

3.4 | A characteristic angle

To quantify the observation from the cluster analysis, which showed a massive change in the relative orientation of the two subunits, we define a characteristic dimer angle using the following three atoms: Cα of $G27_A$, Cu(I), and Cα of $G27_B$. The residue chosen for this purpose, G27, is the C-cap of the large helix, while the Cu(I) is located near the N-terminus of this helix. The resultant angle should approximate the relative orientation of the protein dimers. The plots of the dimer angle as a function of time are shown in Figure 4.

The behavior of the dimer angle as a function of time mirrors that seen in the RMSD plots: monotonous for the 4-coordinated replicas, larger fluctuations for the 3-coordinated replicas, and a wide range of values for the 2-coordinated replicas that sometimes converge to a new, consistent value (~60° for CHARMM36m; ~80° or ~100° for some AMBER-SB14 replicas).

3.5 | Comparison with DEER distance distributions

Comparison between DEER distances and MD simulations is useful for elucidating the structural features of biomacromolecules.[13,35,40–42] Several distance distributions between selected labeled positions were reported.[2,9,10] The spin label was MTSL (S-[1-oxyl-2,2,5,5-tetramethyl-2,5-dihydro-1H-pyrrol-3-yl]methyl methanesulfonothioate) which is characterized by its long, flexible tether. A dummy atom analog, which was parametrized to mimic the motion of the spin label, is available via the

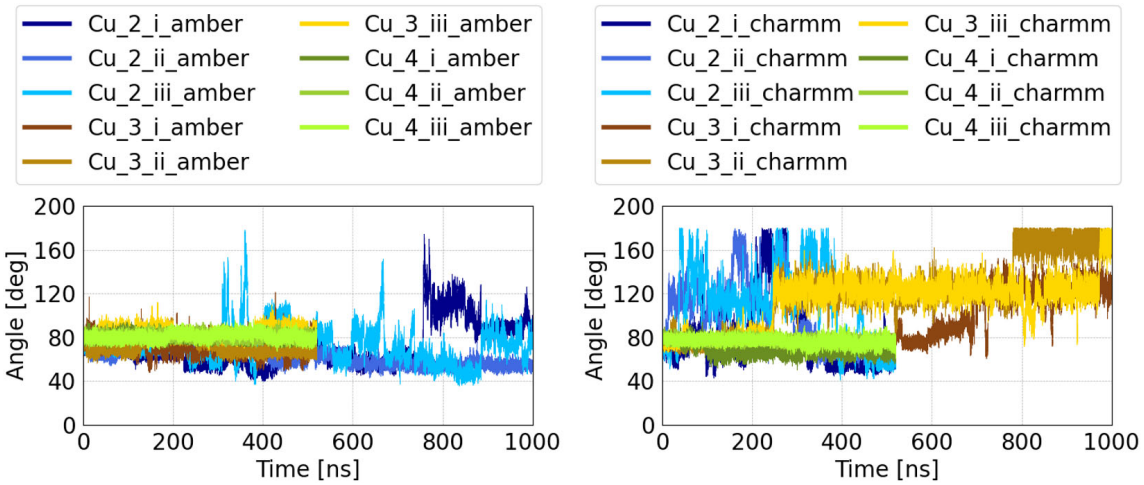

FIGURE 4 Characteristic angle as a function of simulation time. Force fields: AMBER-SB14 (top); CHARMM36m (bottom)

CHARMM-GUI server.[34,35] This server accounts implicitly for the flexibility of side chains around the dummy spin label by means of mutating them to Alanine residues. This way, the initial conformation (rotamer) should not restrict the motion of the dummy spin label. Representative conformations (an instantaneous conformation most similar to the average structure of a cluster) were uploaded to the server and labeled at suitable positions to mimic the experimental settings. After a short MD simulation (see Methods section for a detailed description) the distance distributions between the spin labels were calculated. For some conformations, especially for the open conformations typical to the lower coordination states, there was not a good agreement with some experimental data. The results for representative structures that are comparable to the experimental distributions are presented in Figure 5 and in Table S4. For cartoon representations of some of the relevant conformations, see Figure 3.

In general, the 4-coordinated state is similar to the crystal structure and in agreement with most DEER distributions assigned to the closed state. The open conformations observed in the lower coordination states can fit distributions with lower probability in the DEER distance distribution spectra.

In most cases, the computed and experimental distance distributions between positions $K25C_A$ – $K25C_B$ agree (~2 nm). One exception is found for the extended state (3-coordinated, distribution ~3 nm), although it matches a smaller peak in the spectrum. An additional exception is found for the inverted conformation, which possesses a distribution at ~5 nm, which is close to the detection limit under the experimental conditions. This distribution may fit a minor peak in the experimental spectra with significant uncertainty associated with it. Similarly, the distributions between $K38C_A$ – $K38C_B$ are similar for the simulations and experiment. (~2 nm).

In the case of $T61C_A$ – $T61C_B$, the spin label is located on a terminus of a β-sheet near a flexible loop. Hence, the exact experimental orientation might be challenging to predict and reproduce computationally. Whereas experimentally the labels were measured to be 24 ± 4 Å apart, most computed values range from 31 to 38 Å, although a smaller peak corresponding to this latter distribution was reported experimentally.

The distribution between $C41_A$ – $C41_B$ was reported to contain two main distributions: 41 ± 3 and 27 ± 6 Å. In most cases, the computed distribution is a bit higher than the ~4 nm peak, at 47–49 Å, which, as mentioned earlier is close to the detection limit. However, some twisted conformations are in good agreement with the ~4 nm peak and the inverted conformation matches the ~2.5 nm peak.

To conclude, the 4-coordination state replicas exhibit rigid behavior with conformations similar to the crystal structure (Cα RMSD < 5 Å), while the 3-coordinated state exhibits intermediate flexibility. The 2-coordinated states exhibit a wide range of conformations, suggesting elevated flexibility, and several of these open conformations are in agreement with DEER data. We ascribe this correlation between metal coordination state and protein flexibility to an anchoring role played by Cys-copper interactions. The Cys-copper interactions keep the local network of interactions between the monomers intact, and loss of these interactions lead to the increased flexibility of the two Atox1 monomers. This is clearly reflected in the characteristic angle defined between the two monomers (Figures 4 and S3D).

4 | CONCLUSIONS

The human metallochaperone Atox1 takes part in copper ion transportation and is responsible for cellular copper

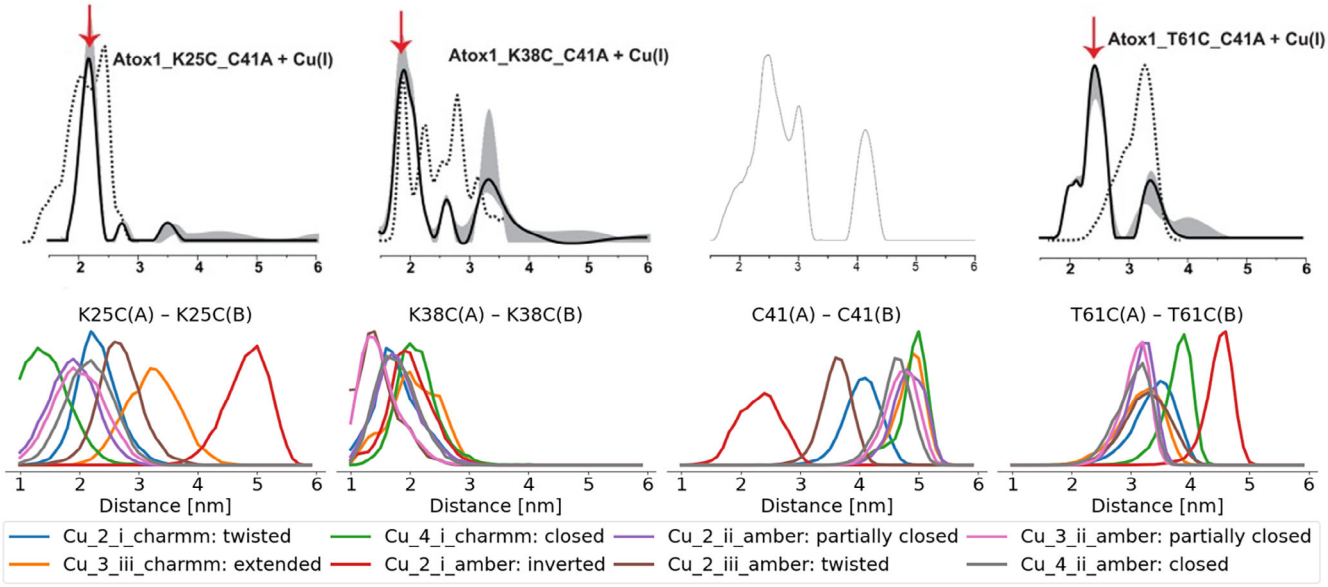

FIGURE 5 Experimental and simulated double electron–electron resonance (DEER) distributions of some key conformations. Upper panel: Experimental results (taken from Reference 9 with permission from the Protein Society). The solid line is the distribution and the grey shadow is the error. The dotted line was simulated in the mentioned work and is not further discussed here. Lower panel: simulated distance distributions from the current work. Blue: Cu_2_i_charmm, twisted; Orange: Cu_3_iii_charmm, extended; Green: Cu_4_i_charmm, closed; Red: Cu_2_i_amber, inverted; Purple: Cu_2_ii_amber, partially closed; Brown: Cu_2_iii_amber, twisted; Pink: Cu_3_ii_amber, partially closed; Grey: Cu_4_ii_amber, closed

metabolism. For efficient transportation it should be able to bind the ions tightly while diffusing and release them upon reaching the target. In a previous QM/MM study, we observed changes in the coordination state of the Cu(I) ions, switching between 3- and 4-coordination states. A 2-coordinated state was rarely seen, likely due to the limited timescale of these simulations. Here, we aimed to explore the three coordination states for longer simulation periods than can be reached with standard QM/MM MD simulations. To this end, we developed FF parameters for Cys-Cu(I) binding and performed brute-force MM MD simulations. We noticed an increase in the flexibility of the two monomers with a decrease in coordination number.

To assess the conformational changes during the simulations, RMSD and RMSF values with respect to the initial structure (X-ray based) were calculated. The RMSD and RMSF values tend to increase with a decrease in coordination number. The elevated RMSD and RMSF values, which arise from enhanced flexibility around the copper hinge, allow the protein to adopt many conformations.

Cluster analysis of the instantaneous conformations revealed a wealth of states for the 2- and 3-coordination states, but only a few conformations for the 4-coordinated state. Predicted DEER distributions of the observed conformations mostly agree with experimental DEER data, with some matching the major peaks, others minor peaks, while some computationally observed distance distributions were beyond the experimental detection limits.

In conclusion, we hypothesize that the multiple states observed for Atox1 in its low coordination states may allow it to interact with other Cu-binding proteins to facilitate metal ion transport. Further experiments are required to establish this hypothesis.

AUTHOR CONTRIBUTIONS

Renana Schwartz: Data curation (equal); formal analysis (equal); investigation (equal). **Sharon Ruthstein:** Resources (equal); supervision (equal). **Dan Thomas Major:** Resources (equal); supervision (equal).

ACKNOWLEDGMENT

This work was supported by the Israel Science Foundation (Grant # 1683/18).

DATA AVAILABILITY STATEMENT

Data available on request from the authors.

ORCID

Renana Schwartz https://orcid.org/0000-0003-0552-6434

Sharon Ruthstein https://orcid.org/0000-0002-1741-6892

Dan Thomas Major https://orcid.org/0000-0002-9231-0676

REFERENCES

1. Hunsaker EW, Franz KJ. Emerging opportunities to manipulate metal trafficking for therapeutic benefit. Inorg Chem. 2019;58:13528–13545.
2. Shenberger Y, Shimshi A, Ruthstein S. EPR spectroscopy shows that the blood carrier protein, human serum albumin, closely interacts with the N-terminal domain of the copper transporter, Ctr1. J Phys Chem B. 2015;119:4824–4830.
3. Stefaniak E, Płonka D, Drew SC, et al. The N-terminal 14-mer model peptide of human Ctr1 can collect Cu (II) from albumin. Implications for copper uptake by Ctr1. Metallomics. 2018;10:1723–1727.
4. Klomp LW, Lin S-J, Yuan DS, Klausner RD, Culotta VC, Gitlin JD. Identification and functional expression of HAH1, a novel human gene involved in copper homeostasis. J Biol Chem. 1997;272:9221–9226.
5. Wernimont AK, Huffman DL, Lamb AL, O'Halloran TV, Rosenzweig AC. Structural basis for copper transfer by the metallochaperone for the Menkes/Wilson disease proteins. Nat Struct Biol. 2000;7:766–771.
6. Flores AG, Unger VM. Atox1 contains positive residues that mediate membrane association and aid subsequent copper loading. J Membr Biol. 2013;246:903–913.
7. Robinson NJ, Winge DR. Copper metallochaperones. Annu Rev Biochem. 2010;79:537–562.
8. O'Halloran TV, Culotta VC. Metallochaperones, an intracellular shuttle service for metal ions. J Biol Chem. 2000;275:25057–25060.
9. Levy AR, Turgeman M, Gevorkyan-Aiapetov L, Ruthstein S. The structural flexibility of the human copper chaperone Atox1: Insights from combined pulsed EPR studies and computations. Protein Sci. 2017;26:1609–1618.
10. Perkal O, Qasem Z, Turgeman M, et al. Cu (I) controls conformational states in human Atox1 metallochaperone: An EPR and multiscale simulation study. J Phys Chem B. 2020;124:4399–4411.
11. Ansbacher T, Chourasia M, Shurki A. Copper-chaperones with dicoordinated Cu (I)—Unique protection mechanism. Proteins. 2013;81:1411–1419.
12. Ansbacher T, Shurki A. Predicting the coordination number within copper chaperones: Atox1 as case study. J Phys Chem B. 2012;116:4425–4432.
13. Schwartz R, Ruthstein S, Major DT. Molecular dynamics simulations of the Apo and Holo States of the copper binding protein CueR reveal principal bending and twisting motions. J Phys Chem B. 2021;125:9417–9425.
14. Casto J, Mandato A, Hofmann L, et al. Cu (ii)-based DNA labeling identifies the structural link between transcriptional activation and termination in a metalloregulator. Chem Sci. 2022;13:1693–1697.
15. Shoshan MS, Dekel N, Goch W, et al. Unbound position II in MXCXXC metallochaperone model peptides impacts metal binding mode and reactivity: Distinct similarities to whole proteins. J Inorg Biochem. 2016;159:29–36.
16. MacKerell AD Jr, Bashford D, Bellott M, et al. All-atom empirical potential for molecular modeling and dynamics studies of proteins. J Phys Chem B. 1998;102:3586–3616.
17. Huang J, MacKerell AD Jr. CHARMM36 all-atom additive protein force field: Validation based on comparison to NMR data. J Comput Chem. 2013;34:2135–2145.
18. Huang J, Rauscher S, Nawrocki G, et al. CHARMM36m: An improved force field for folded and intrinsically disordered proteins. Nat Methods. 2017;14:71–73.
19. Maier JA, Martinez C, Kasavajhala K, Wickstrom L, Hauser KE, Simmerling C. ff14SB: Improving the accuracy of protein side chain and backbone parameters from ff99SB. J Chem Theory Comput. 2015;11:3696–3713.
20. Brooks BR, Bruccoleri RE, Olafson BD, States DJ, Sa S, Karplus M. CHARMM: A program for macromolecular energy, minimization, and dynamics calculations. J Comput Chem. 1983;4:187–217.
21. Brooks BR, Brooks CL III, Mackerell AD Jr, et al. CHARMM: The biomolecular simulation program. J Comput Chem. 2009;30:1545–1614.
22. Phillips JC, Braun R, Wang W, et al. Scalable molecular dynamics with NAMD. J Comput Chem. 2005;26:1781–1802.
23. Phillips JC, Hardy DJ, Maia JD, et al. Scalable molecular dynamics on CPU and GPU architectures with NAMD. J Chem Phys. 2020;153:044130.
24. Pitts AL, Hall MB. Investigating the electronic structure of the Atox1 copper (I) transfer mechanism with density functional theory. Inorg Chem. 2013;52:10387–10393.
25. Frisch MJ, Trucks GW, Schlegel HB, et al. Gaussian 16 Rev. A.03. (2016). Wallingford, CT.
26. Woon DE, Dunning TH Jr. Gaussian basis sets for use in correlated molecular calculations. III. The atoms aluminum through argon. J Chem Phys. 1993;98:1358–1371.
27. Møller C, Plesset MS. Note on an approximation treatment for many-electron systems. Phys Rev. 1934;46:618–622.
28. Frisch MJ, Head-Gordon M, Pople JA. A direct MP2 gradient method. Chem Phys. 1990;166:275–280.
29. Knapp B, Ospina L, Deane CM. Avoiding false positive conclusions in molecular simulation: The importance of replicas. J Chem Theory Comput. 2018;14:6127–6138.
30. Ewald PP. Die Berechnung optischer und elektrostatischer Gitterpotentiale. Ewald summation Ann Phys. 1921;369:253–287.
31. Ma Q, Izaguirre JA, Skeel RD. Verlet-I/r-RESPA/impulse is limited by nonlinear instabilities. SIAM J Sci Comput. 2003;24:1951–1973.
32. Bhandarkar M, Brunner R, Chipot C, et al. NAMD User's Guide Urbana. 2003;51:61801.
33. Grant BJ, Rodrigues AP, ElSawy KM, McCammon JA, Caves LS. Bio3d: An R package for the comparative analysis of protein structures. Bioinformatics. 2006;22:2695–2696.
34. Jo S, Kim T, Iyer VG, Im W. CHARMM-GUI: A web-based graphical user interface for CHARMM. J Comput Chem. 2008;29:1859–1865.
35. Qi Y, Lee J, Cheng X, et al. CHARMM-GUI DEER facilitator for spin-pair distance distribution calculations and preparation of restrained-ensemble molecular dynamics simulations. J Comput Chem. 2020;41:415–420.
36. Harris CR, Millman KJ, van der Walt SJ, et al. Array programming with NumPy. Nature. 2020;585:357–362.
37. Turner M, Mutter ST, Platts JA. Molecular dynamics simulation on the effect of transition metal binding to the N-terminal fragment of amyloid-β. J Biomol Struct Dyn. 2019;37:4590–4600.
38. Ortega M, Vilhena J, Zotti LA, Díez-Pérez I, Cuevas JC, Pérez R. Tuning structure and dynamics of blue copper azurin junctions via single amino-acid mutations. Biomolecules. 2019;9:611.

39. Orädd F, Steffen JH, Gourdon P, Andersson M. Copper binding leads to increased dynamics in the regulatory N-terminal domain of full-length human copper transporter ATP7B. PLoS Comput Biol. 2022;18:e1010074.
40. Islam SM, Stein RA, Mchaourab HS, Roux B. Structural refinement from restrained-ensemble simulations based on EPR/-DEER data: Application to T4 lysozyme. J Phys Chem B. 2013; 117:4740–4754.
41. Hays JM, Boland E, Kasson PM. Inference of joint conformational distributions from separately acquired experimental measurements. J Phys Chem Lett. 2021;12:1606–1611.
42. Sarver JL, Townsend JE, Rajapakse G, Jen-Jacobson L, Saxena S. Simulating the dynamics and orientations of spin-labeled side chains in a protein–DNA complex. J Phys Chem B. 2012;116:4024–4033.

SUPPORTING INFORMATION

Additional supporting information can be found online in the Supporting Information section at the end of this article.

How to cite this article: Schwartz R, Ruthstein S, Major DT. Copper coordination states affect the flexibility of copper Metallochaperone Atox1: Insights from molecular dynamics simulations. Protein Science. 2022;31(12):e4464. https://doi.org/10.1002/pro.4464